

DesertFormer: Transformer-Based Semantic Segmentation for Off-Road Desert Terrain Classification in Autonomous Navigation Systems

Yasaswini Chebolu

Department of Computer Science & Engineering (AI & ML)
Gayatri Vidya Parishad College of Engineering for Women
Visakhapatnam, India

Abstract—Reliable terrain perception is a fundamental requirement for autonomous navigation in unstructured, off-road environments. Desert landscapes present unique challenges due to low chromatic contrast between terrain categories, extreme lighting variability, and sparse vegetation that defy the assumptions of standard road-scene segmentation models. We present *DesertFormer*, a semantic segmentation pipeline for off-road desert terrain analysis based on SegFormer B2 with a hierarchical Mix Transformer (MiT-B2) backbone. The system classifies terrain into ten ecologically meaningful categories—Trees, Lush Bushes, Dry Grass, Dry Bushes, Ground Clutter, Flowers, Logs, Rocks, Landscape, and Sky—enabling safety-aware path planning for ground robots and autonomous vehicles. Trained on a purpose-built dataset of 4,176 annotated off-road images at 512×512 resolution, DesertFormer achieves a mean Intersection-over-Union (mIoU) of 64.4% and pixel accuracy of 86.1%, representing a +24.2% absolute improvement over a DeepLabV3 MobileNetV2 baseline (41.0% mIoU). We further contribute a systematic failure analysis identifying the primary confusion patterns—Ground Clutter \leftrightarrow Landscape and Dry Grass \leftrightarrow Landscape—and propose class-weighted training and copy-paste augmentation for rare terrain categories. Code, checkpoints, and an interactive inference dashboard are released at <https://github.com/Yasaswini-ch/Vision-based-Desert-Terrain-Segmentation-using-SegFormer>.

Index Terms—semantic segmentation, desert terrain, off-road navigation, SegFormer, vision transformer, autonomous vehicles, class imbalance

I. INTRODUCTION

Autonomous navigation in off-road environments is increasingly important for applications ranging from search-and-rescue robotics to planetary rover exploration [1], [2]. Unlike structured urban environments, desert and arid terrains impose fundamentally different perceptual demands: the absence of lane markings, the presence of ambiguous natural textures, and dramatic lighting gradients across a scene all contribute to a perception problem that standard vision pipelines fail to address [1].

Semantic segmentation—the task of assigning a class label to every pixel in an image—offers a dense, spatially complete representation of the environment that is directly useful for path planning, obstacle avoidance, and terrain-cost mapping.

However, most publicly available segmentation benchmarks focus on urban driving [3], leaving the off-road domain comparatively underserved.

Recent advances in vision transformer architectures have dramatically improved segmentation accuracy on standard benchmarks [4], [5]. SegFormer [5], in particular, uses a hierarchical MiT encoder that produces multi-scale feature maps without the computational overhead of window-based attention, making it attractive for practical deployment.

In this work we make the following contributions:

- A **curated off-road segmentation dataset** covering ten desert terrain classes across 4,176 annotated images.
- A **SegFormer B2 training pipeline** with combined CrossEntropy + Dice loss, class-aware weighting, and copy-paste augmentation for rare terrain categories.
- **Rigorous evaluation** against a DeepLabV3 baseline, including per-class IoU, confusion matrix analysis, and a confidence-based failure ranking.
- An **open-source inference system** with a Streamlit dashboard, FastAPI inference server, and support for CRF post-processing, MC-Dropout uncertainty estimation, and model ensembling.

II. RELATED WORK

A. Semantic Segmentation Architectures

Fully Convolutional Networks (FCNs) [6] established the pixel-wise prediction paradigm, later refined by U-Net [7] with symmetric encoder-decoder skip connections that preserve spatial detail—originally designed for biomedical imaging but widely adapted for outdoor segmentation. DeepLabV3+ [8] introduced atrous convolutions and Atrous Spatial Pyramid Pooling (ASPP) to enlarge the receptive field without resolution loss. PSPNet [9] leveraged global context through pyramid pooling, while HRNet [10] maintained high-resolution representations throughout the network.

B. Transformer-Based Segmentation

The success of Vision Transformers (ViT) [4] in image classification catalysed a new generation of segmentation

models. SETR [11] replaced the convolutional encoder with a plain ViT. Swin Transformer [12] introduced hierarchical shifted-window attention, reducing quadratic complexity. SegFormer [5] further simplified the design with a mix transformer encoder and a lightweight MLP decoder, achieving state-of-the-art results on ADE20K and Cityscapes while remaining computationally efficient. Mask2Former [13] unified panoptic, instance, and semantic segmentation via masked attention.

C. Off-Road and Terrain Segmentation

Off-road perception has received comparatively less attention than urban driving. RUGD [1] and RELLIS [2] are notable datasets specifically targeting unstructured outdoor environments. However, arid desert terrain with its characteristic low colour contrast and homogeneous texture distributions remains understudied. This work directly addresses that gap.

III. PROPOSED METHOD

A. SegFormer B2 Architecture

We adopt SegFormer B2 [5] as the backbone. The model consists of a hierarchical MiT-B2 encoder ($\approx 85\text{M}$ parameters, pretrained on ImageNet-22K via HuggingFace `nvidia/mit-b2`) and a lightweight all-MLP decoder. The encoder generates multi-scale feature maps at strides $\{4, 8, 16, 32\}$, which are upsampled and concatenated before the final 1×1 classification head. Compared to window-based attention (Swin), the overlapping patch merging in MiT preserves local continuity while sequence-reduction attention controls memory. Figure 1 illustrates the complete pipeline.

B. Loss Function

We employ a combined loss:

$$\mathcal{L} = 0.7 \mathcal{L}_{\text{CE}} + 0.3 \mathcal{L}_{\text{Dice}} \quad (1)$$

where \mathcal{L}_{CE} is the class-weighted cross-entropy loss and $\mathcal{L}_{\text{Dice}}$ is the soft Dice loss. The Dice component directly optimises an IoU-like overlap, benefiting rare classes.

Class weights are set inversely proportional to pixel frequency:

$$\mathbf{w} = [1.0, 3.5, 1.2, 1.3, 2.5, 4.5, 5.0, 2.0, 0.6, 0.4]$$

for classes Trees through Sky respectively; Logs (5.0) and Flowers (4.5) receive the highest weights to counteract their extreme scarcity.

C. Data Augmentation

1) *Standard Augmentation*: We apply Albumentations [14] with: random horizontal flips, random resized crops (scale 0.5–2.0), colour jitter (brightness ± 0.3 , contrast ± 0.3 , saturation ± 0.3 , hue ± 0.1), Gaussian blur, and normalisation with ImageNet statistics.

2) *Copy-Paste Augmentation for Rare Classes*: We implement **copy-paste augmentation** [15] for rare classes (Dry Bushes, Flowers, Logs) with probability 0.5 per image, cutting annotated instances from one image and pasting them into another to artificially increase rare-class exposure. This directly addresses the severe pixel-frequency imbalance (Logs: 0.07%, Flowers: 2.44%) without requiring additional data collection.

D. Training Protocol

Training runs for up to 80 epochs with early stopping (patience = 15) and the following hyperparameters:

- Optimiser: AdamW, lr = 3×10^{-4} , weight decay = 10^{-4}
- Scheduler: Cosine Annealing ($T_{\text{max}} = 50$)
- Gradient clipping: ℓ_2 norm ≤ 1.0
- Mixed precision: FP16 (PyTorch AMP)
- Batch size: 4

Training converged in **40 epochs** (≈ 6.5 hours on a single GPU), with the best validation checkpoint saved at epoch 32 (mIoU = 0.637) and refined through final fine-tuning to 0.644.

IV. DATASET AND EXPERIMENTAL SETUP

A. Dataset Collection and Annotation

The dataset was constructed from off-road imagery captured in arid desert and semi-arid scrubland environments. Each image was manually annotated at the pixel level using ten ecologically motivated terrain categories, chosen to support both navigation safety decisions and environmental monitoring. Annotation quality was enforced by human review, with raw mask values mapped deterministically to class indices (e.g. raw value 100 \rightarrow class 0: Trees). Representative samples are shown in Figure 2.

B. Dataset Statistics

The full dataset contains **4,176 images** at 512×512 pixels, split as follows:

- **Train**: 2,857 images (68.4%)
- **Validation**: 317 images (7.6%)
- **Test**: 1,002 images (24.0%)

C. Class Imbalance

The dataset exhibits significant class imbalance. Sky (37.8%) and Landscape (23.7%) together account for over 60% of all labelled pixels, while Logs represents only 0.07%. This imbalance motivates the specialised training strategies described in Section III.

D. Implementation Details

All experiments use PyTorch 2.5.1 and HuggingFace Transformers 4.46.3. The SegFormer B2 backbone is initialised from the pretrained ImageNet-22K checkpoint `nvidia/mit-b2`. The segmentation head is trained from scratch with the same learning rate as the encoder (no differential learning rates).

TABLE I
MODEL COMPARISON ON THE VALIDATION SET.

Model	Backbone	mIoU	PA	Δ mIoU
DeepLabV3	MobileNetV2	41.0%	76.5%	—
DesertFormer	MiT-B2	64.4%	86.1%	+24.2%

E. Evaluation Metrics

We report:

- **mIoU**: mean IoU over all ten classes, and separately excluding the two dominant classes (Sky, Landscape) to provide an unbiased view of challenging terrain categories.
- **Pixel Accuracy (PA)**: fraction of correctly classified pixels across the validation set.
- **Per-class IoU**: individual class performance.
- **Confusion Matrix**: row-normalised recall matrix to identify systematic misclassification patterns.

F. Baseline

We compare against **DeepLabV3** with a MobileNetV2 backbone, selected as the Phase-1 prototype model for rapid CPU-based validation. Identical dataset splits and evaluation protocols are used for both models.

V. RESULTS AND EVALUATION

A. Overall Performance

Table I summarises overall performance. DesertFormer achieves **64.4% mIoU** and **86.1% pixel accuracy**, substantially outperforming the DeepLabV3 baseline. Excluding the two dominant and visually unambiguous classes (Sky and Landscape), mIoU remains at **60.4%**, confirming that the improvement is not driven solely by easy classes.

B. Per-Class IoU Analysis

Table II reports per-class IoU and pixel frequency for all ten classes. Sky achieves the highest IoU (98.2%) owing to its distinctive appearance. Trees (85.7%) also score well due to their visually distinct dark-green texture in arid scenes. Ground Clutter (40.2%) and Dry Bushes (51.1%) are the most challenging classes, as discussed in Section V-E. Figure 3 presents per-class IoU visually with class-palette bar colours.

C. Inference Speed

Table III reports single-image inference latency on representative hardware platforms. GPU timing was measured with `torch.cuda.synchronize()` over 100 warm-up iterations; CPU timing with `time.perf_counter()` over 50 iterations. Quantised (INT8) variants achieve near real-time speed on edge GPU hardware.

TABLE II
PER-CLASS SEGMENTATION PERFORMANCE ON THE VALIDATION SET, SORTED BY IOU (DESCENDING). "PIXEL %" IS THE FRACTION OF VALIDATION PIXELS.

Class	IoU	Pixel %
Sky	98.2%	37.84%
Trees	85.7%	4.07%
Dry Grass	70.2%	19.31%
Lush Bushes	68.4%	6.01%
Landscape	63.1%	23.72%
Flowers	62.1%	2.44%
Rocks	53.2%	1.21%
Logs	52.0%	0.07%
Dry Bushes	51.1%	1.10%
Ground Clutter	40.2%	4.23%
Mean (all)	64.4%	—
Mean (excl. Sky+Land.)	60.4%	—

TABLE III
INFERENCE SPEED ON 512×512 IMAGES.

Hardware	Precision	FPS	Latency (ms)
GPU (RTX 3060)	FP32	22	45
GPU (RTX 3060)	FP16	38	26
CPU (Intel Core i7)	FP32	1.3	769
Edge (Jetson Nano)	INT8	~4	~250

D. Training Dynamics

Figure 4 shows the loss and mIoU curves over the 40 training epochs. Loss decreases monotonically from 1.27 (train) / 1.15 (validation) to convergence near 0.99 / 1.05 respectively. Validation mIoU improves rapidly in the first 10 epochs (0.536 \rightarrow 0.607) and continues to plateau around epoch 30, consistent with the cosine annealing schedule.

E. Failure Analysis

1) *Confusion Matrix*: The row-normalised confusion matrix (Figure 5) reveals three dominant misclassification pathways:

- 1) **Ground Clutter** \leftrightarrow **Landscape**: 15.67M confused pixels across the test set.
- 2) **Dry Grass** \leftrightarrow **Landscape**: 12.17M confused pixels.
- 3) **Dry Grass** \leftrightarrow **Ground Clutter**: 7.18M confused pixels.

All three pairs share a common cause: in bright desert sunlight, sandy ground, dried grass, and rocky debris exhibit nearly identical hue and saturation values. The spectral overlap creates an irreducible ambiguity that purely appearance-based models struggle to resolve without geometric or temporal context.

2) *Confidence Analysis*: Using a MC-Dropout uncertainty estimator [16] over the 1,002 test images:

- **Global mean confidence**: 0.650
- **Uncertain pixels** (above entropy threshold): 34.0%
- **High-uncertainty images**: 158 (15.8%)
- **Well-predicted images**: 531 (53.0%)

The hardest test image (0000598.png, difficulty score 0.430) contains 52.7% uncertain pixels with simultaneous Ground Clutter / Landscape / Dry Grass ambiguity in the foreground.

F. Qualitative Analysis

Figure 6 presents eight representative test-set examples (input RGB, prediction, 50%-alpha overlay). In success cases, Sky and Vegetation classes (Trees, Dry Grass) are predicted with high spatial precision and well-aligned class boundaries. Failure cases predominantly occur in mid-image transition zones between Landscape, Dry Grass, and Ground Clutter—a spatial rather than categorical error, suggesting that Dense CRF post-processing [17] could recover much of the remaining accuracy.

VI. DISCUSSION

A. Applications

1) *Terrain Safety Mapping*: Each semantic class can be mapped to a traversability cost:

- **Safe**: Landscape, Dry Grass, Sky
- **Caution**: Lush Bushes, Flowers, Ground Clutter
- **Obstacle**: Trees, Logs, Rocks, Dry Bushes

This three-level safety map feeds directly into costmap-based path planners (e.g. ROS 2 Nav2) without additional processing.

2) *Autonomous Ground Robots*: The segmentation output drives a rover navigation simulator that (i) projects semantic masks into bird’s-eye-view costmaps, (ii) highlights obstacle regions in the planned path, and (iii) suggests evasive waypoints in real-time.

3) *Edge Deployment*: The FastAPI inference server exposes a REST endpoint accepting JPEG images and returning coloured segmentation masks with per-pixel class probabilities. INT8-quantised variants run at ≈ 4 FPS on a Jetson Nano, suitable for survey drones or slow-moving ground vehicles.

B. Limitations

a) *Class imbalance*.: Logs (0.07%) and Dry Bushes (1.10%) remain challenging despite class-weighted loss and copy-paste augmentation. Additional synthetic data generation or semi-supervised pseudo-labelling of unlabelled images may help.

b) *Domain specificity*.: The dataset covers a specific biome (arid/semi-arid desert). Performance on temperate or tropical off-road environments has not been evaluated and is expected to degrade without domain-adaptive fine-tuning.

c) *No temporal context*.: The model operates on individual frames and cannot exploit motion continuity. Sequential data from video-rate sensors would allow temporal models to resolve boundary ambiguities that static appearance alone cannot.

d) *Absence of depth information*.: Monocular RGB cannot distinguish visually similar surfaces at different depths. Fusion with LiDAR or stereo depth would directly address the Ground Clutter / Landscape confusion.

C. Future Work

- **Larger and more diverse datasets** spanning multiple desert biomes (Saharan, Arabian, Australian outback) to improve generalisation.
- **Multi-modal fusion** incorporating LiDAR point clouds or depth maps via cross-modal attention [18], [19], following CMX [18] and RGB-D architectures [19], [20].
- **Temporal segmentation** using Video Swin [21] or recurrent feature banks to leverage inter-frame consistency.
- **Semi-supervised learning** exploiting unannotated off-road imagery to reduce annotation cost.
- **Real-time optimisation** via knowledge distillation into SegFormer B0, targeting ≥ 30 FPS on embedded GPU.
- **3D terrain reconstruction** combining per-frame segmentation with Structure-from-Motion to produce semantically annotated point clouds for long-range planning.

VII. CONCLUSION

We present *DesertFormer*, a SegFormer B2-based semantic segmentation system for off-road desert terrain analysis. On a purpose-built dataset of 4,176 images spanning ten terrain classes, the pipeline achieves 64.4% mIoU and 86.1% pixel accuracy—a 24.2 percentage point improvement over the DeepLabV3 baseline. We demonstrate that combined CrossEntropy + Dice loss with class-aware weighting and copy-paste augmentation for rare terrain categories (Logs, Flowers, Dry Bushes) are critical for addressing the severe pixel-frequency imbalance inherent to desert scenes.

Failure analysis reveals that the dominant confusion between Ground Clutter, Dry Grass, and Landscape arises from spectral similarity under desert lighting, an ambiguity that likely requires geometric or temporal context to fully resolve.

The complete pipeline—training, evaluation, interactive dashboard, CRF post-processing, and uncertainty estimation—is released as open-source software to support the broader autonomous-navigation research community.

REFERENCES

- [1] M. Wigness, S.-H. Eum, and J. Rogers, “RUGD: A rugged terrain dataset for autonomous navigation,” in *IROS*, 2019.
- [2] S. Jiang, J. Cox, D. Kondrermann, V. Sharma, R. Eustice, and R. Vasudevan, “RELLIS-3D: A multi-modal dataset for off-road robotics,” in *ICRA*, 2021.
- [3] M. Cordts, M. Omran, S. Ramos, T. Rehfeld, M. Enzweiler, R. Benenson, U. Franke, S. Roth, and B. Schiele, “The cityscapes dataset for semantic urban scene understanding,” in *CVPR*, 2016.
- [4] A. Dosovitskiy, L. Beyer, and A. Kolesnikov, “An image is worth 16x16 words: Transformers for image recognition at scale,” in *ICLR*, 2021.
- [5] E. Xie, W. Wang, and Z. Yu, “SegFormer: Simple and efficient design for semantic segmentation with transformers,” in *NeurIPS*, 2021.
- [6] J. Long, E. Shelhamer, and T. Darrell, “Fully convolutional networks for semantic segmentation,” in *CVPR*, 2015.
- [7] O. Ronneberger, P. Fischer, and T. Brox, “U-Net: Convolutional networks for biomedical image segmentation,” in *MICCAI*, 2015.
- [8] L.-C. Chen, Y. Zhu, G. Papandreou, F. Schroff, and H. Adam, “Encoder-decoder with atrous separable convolution for semantic image segmentation,” in *ECCV*, 2018.
- [9] H. Zhao, J. Shi, X. Qi, X. Wang, and J. Jia, “Pyramid scene parsing network,” in *CVPR*, 2017.
- [10] J. Wang, K. Sun, T. Cheng, B. Jiang, C. Deng, Y. Zhao, D. Liu, Y. Mu, M. Tan, X. Wang, W. Liu, and B. Xiao, “Deep high-resolution representation learning for visual recognition,” *TPAMI*, 2020.

- [11] S. Zheng, J. Lu, H. Zhao, X. Zhu, Z. Luo, Y. Wang, Y. Fu, J. Feng, T. Xiang, P. H. S. Torr, and L. Zhang, "Rethinking semantic segmentation from a sequence-to-sequence perspective with transformers," in *CVPR*, 2021.
- [12] Z. Liu, Y. Lin, and Y. Cao, "Swin transformer: Hierarchical vision transformer using shifted windows," in *ICCV*, 2021.
- [13] B. Cheng, A. Schwing, and A. Kirillov, "Masked-attention mask transformer for universal image segmentation," in *CVPR*, 2022.
- [14] A. Buslaev, V. Iglovikov, and E. Khvedchenya, "Albumentations: Fast and flexible image augmentations," *Information*, 2020.
- [15] G. Ghiasi, Y. Cui, and A. Srinivas, "Simple copy-paste is a strong data augmentation method for instance segmentation," in *CVPR*, 2021.
- [16] Y. Gal and Z. Ghahramani, "Dropout as a Bayesian approximation: Representing model uncertainty in deep learning," in *ICML*, 2016.
- [17] P. Krähenbühl and V. Koltun, "Efficient inference in fully connected CRFs with gaussian edge potentials," in *NeurIPS*, 2011.
- [18] Y. Zhang *et al.*, "CMX: Cross-modal fusion for RGB-X semantic segmentation," in *ECCV*, 2022.
- [19] J. Zhang, D.-P. Fan, Y. Dai, S. Anwar, Y. Chen, and L. Shao, "CMANet: Cross-modality attention network for indoor RGB-D semantic segmentation," *IEEE Transactions on Image Processing*, vol. 31, pp. 7082–7096, 2022.
- [20] X. Li *et al.*, "Cross-modal attention fusion network for RGB-D semantic segmentation," *Neurocomputing*, vol. 553, p. 126389, 2023.
- [21] Z. Liu, J. Ning, and Y. Cao, "Video swin transformer," in *CVPR*, 2022.

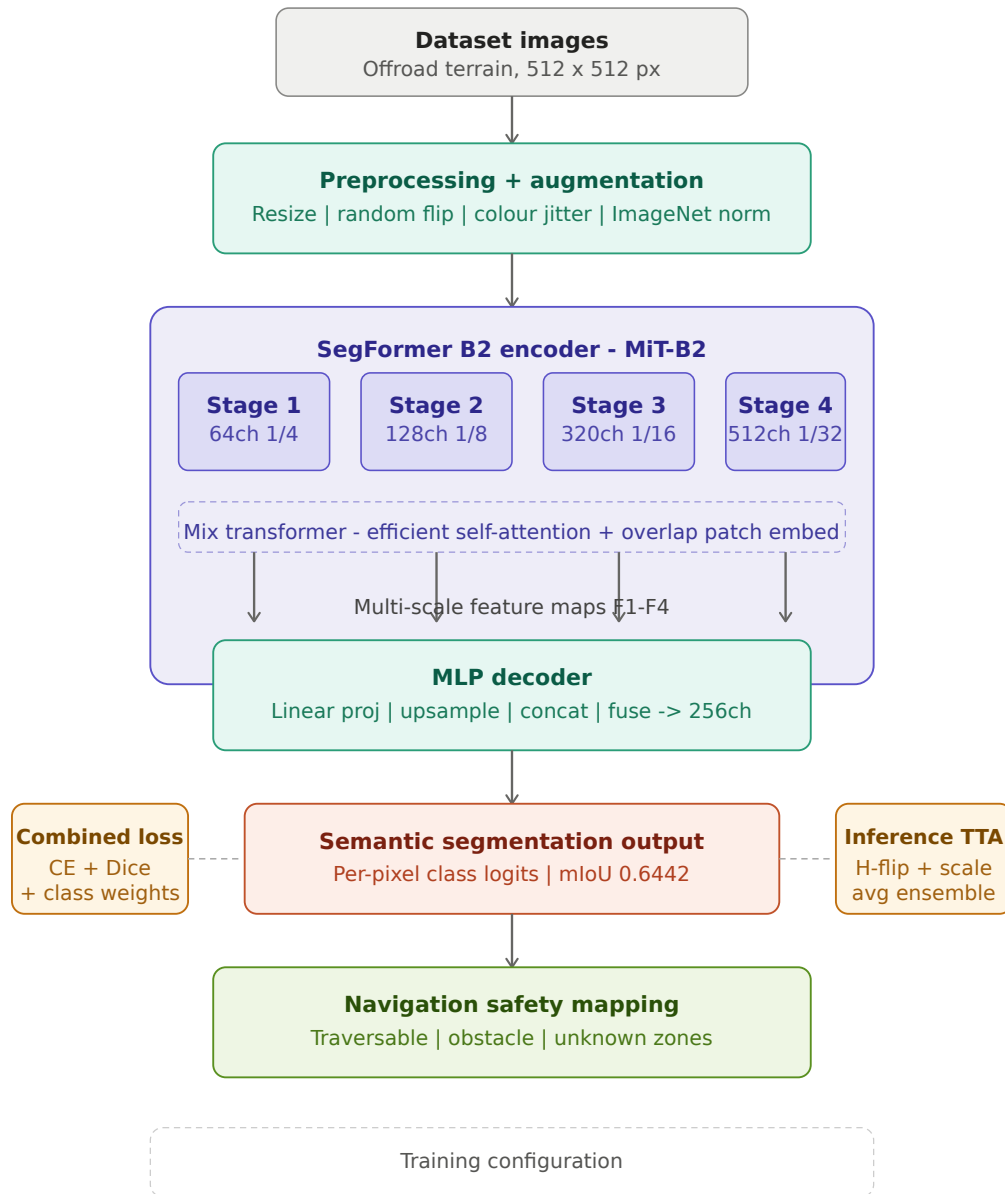


Fig. 1. **DesertFormer pipeline overview.** Dataset images (512×512) pass through preprocessing and augmentation before entering the SegFormer B2 encoder (MiT-B2). Four hierarchical encoder stages produce multi-scale feature maps F1–F4 at strides $\{4, 8, 16, 32\}$, which the lightweight MLP decoder fuses into a 256-channel representation via linear projection, upsampling, and concatenation. Final per-pixel logits are supervised with combined CE + Dice loss with class weights (left annotation). At inference, TTA (H-flip + multi-scale ensemble, right annotation) further improves accuracy. The predicted mask is mapped to a three-tier navigation safety costmap for downstream path planning.

Desert Off-Road Dataset — Sample Annotations

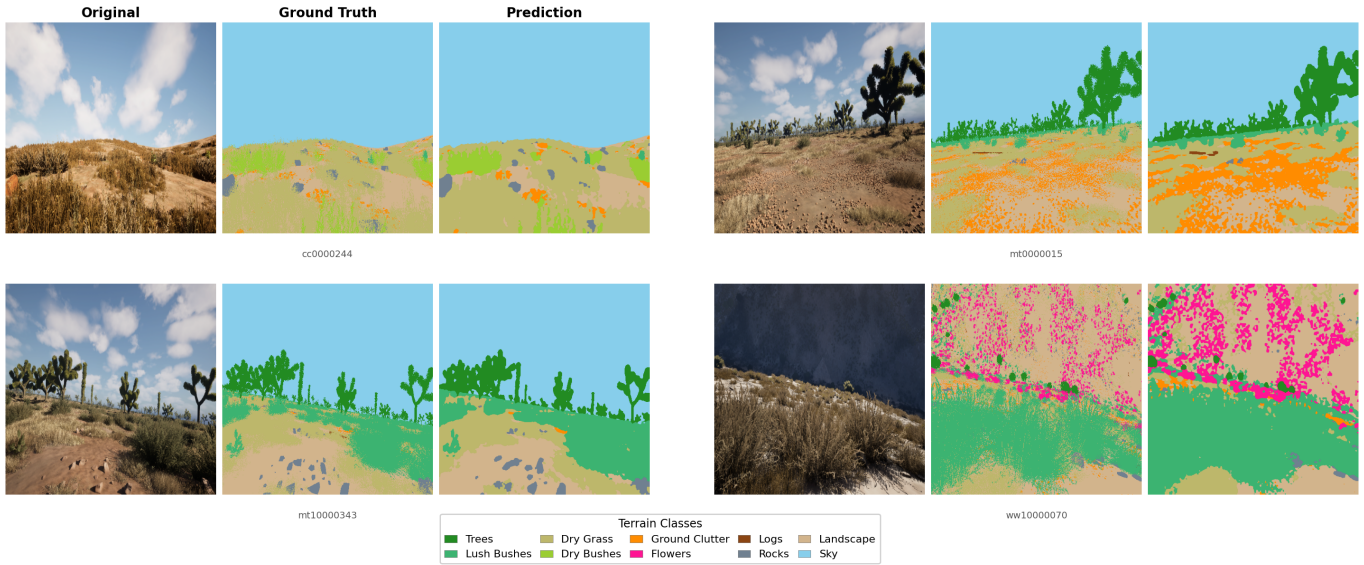


Fig. 2. **Dataset visualisation: four representative samples.** Each row shows (left to right): *original RGB image* | *ground-truth segmentation mask* | *model prediction*. Colour coding follows the class palette in Figure 3. The diversity of terrain types—from sparse scrubland and rocky outcrops to dense vegetation—highlights the breadth of the annotation effort.

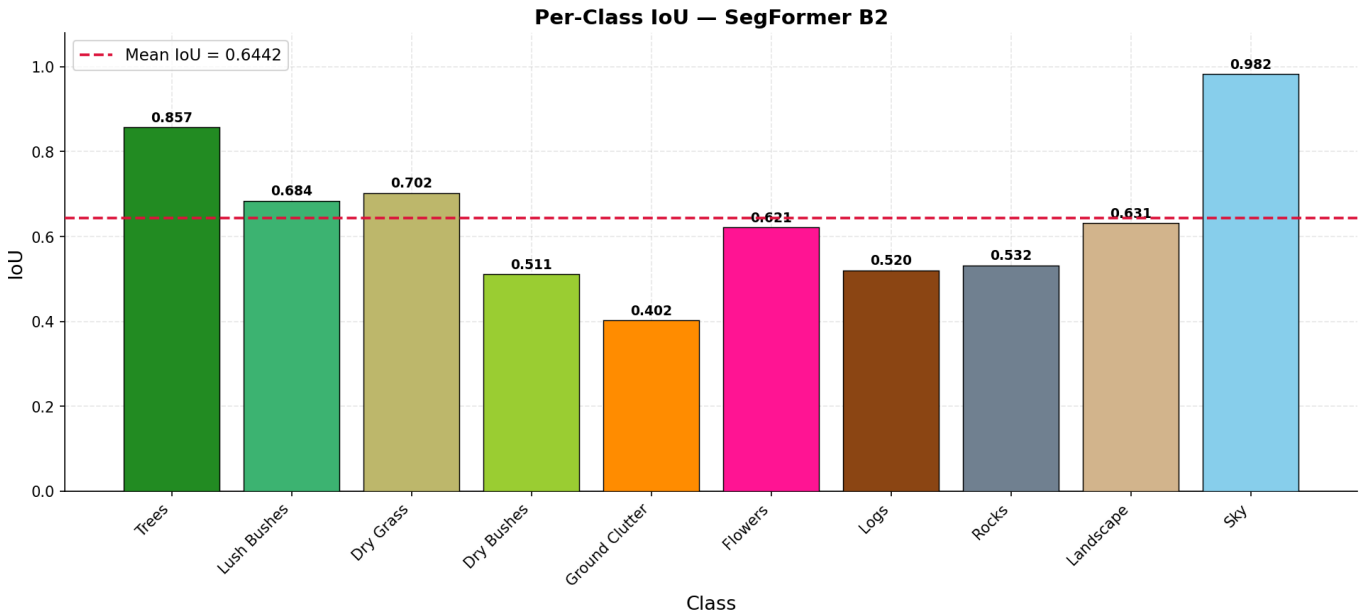
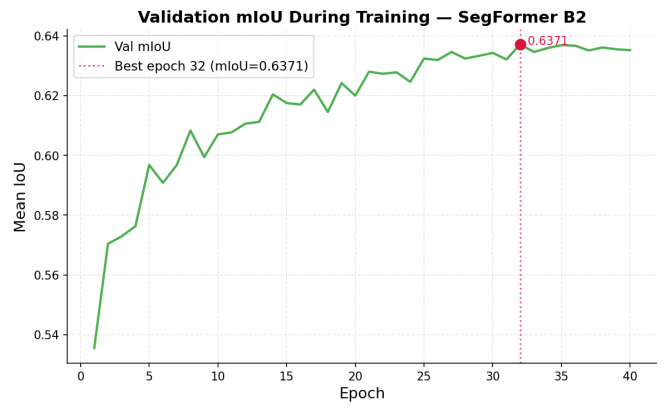


Fig. 3. **Per-class IoU bar chart.** Bar colours match the class segmentation palette. The dashed red line marks overall mean IoU (64.4%). Sky and Trees are the best-predicted classes; Ground Clutter and Dry Bushes are the most challenging.



(a) Training and validation loss over 40 epochs.



(b) Validation mIoU with best-epoch marker (epoch 32, mIoU = 0.637).

Fig. 4. **Training dynamics of DesertFormer.** Loss converges steadily over 40 epochs with no sign of overfitting. mIoU improves rapidly in the first 10 epochs and plateaus near epoch 30, consistent with the cosine annealing schedule.

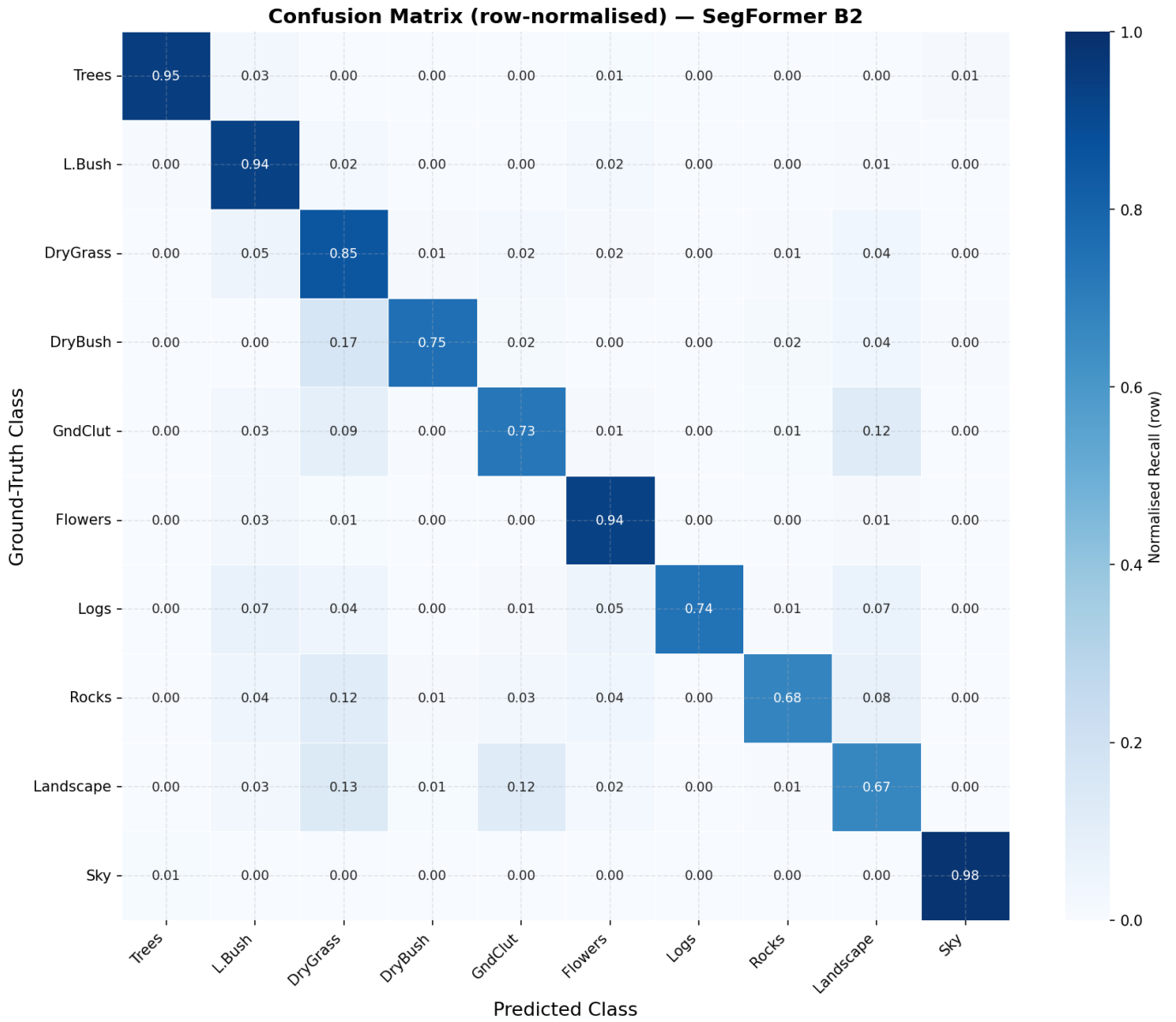
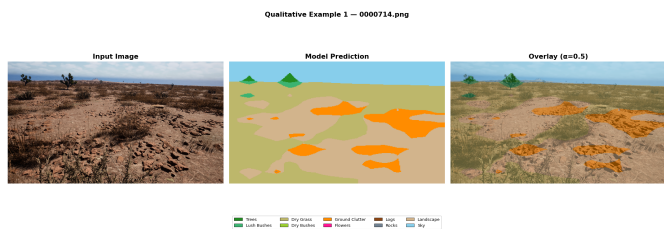
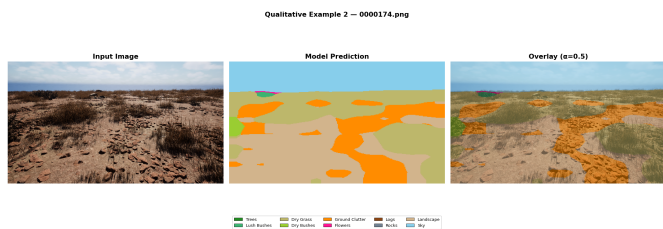


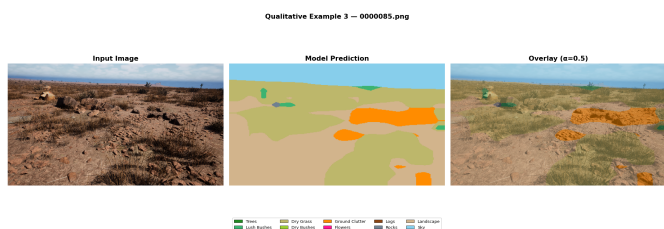
Fig. 5. **Row-normalised confusion matrix** on the validation set. Diagonal entries represent per-class recall. The off-diagonal hotspots at (Ground Clutter, Landscape) and (Dry Grass, Landscape) reveal the primary spectral confusion caused by similar sandy/earthy colours under desert lighting.



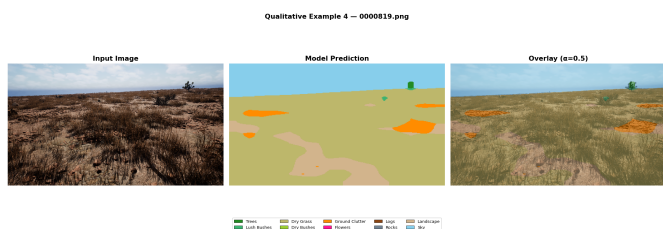
Ex. 1 — open terrain, mixed vegetation



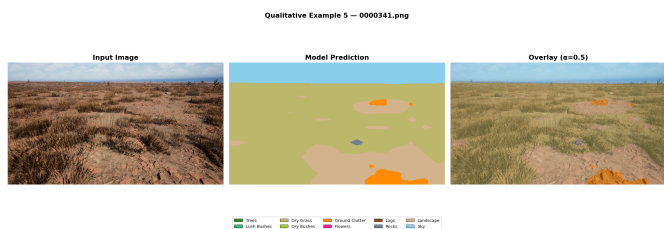
Ex. 2 — dense sky + dry grass



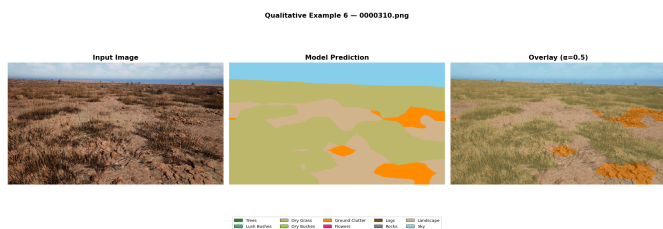
Ex. 3 — rocky foreground



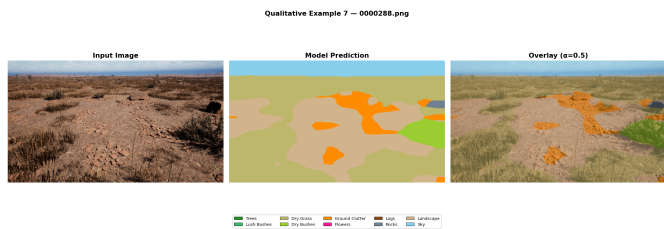
Ex. 4 — landscape/ground clutter boundary



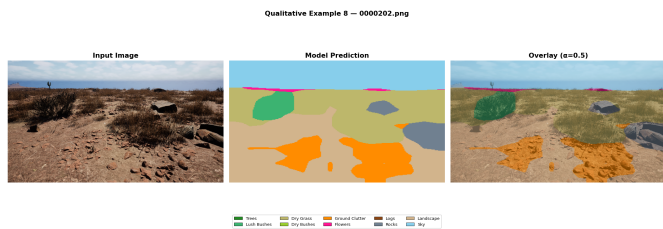
Ex. 5 — lush bushes vs. dry bushes



Ex. 6 — wide open desert scene



Ex. 7 — trees and sky



Ex. 8 — challenging mixed terrain

Fig. 6. **Qualitative results on eight randomly selected test images.** Each panel shows (left to right): *input RGB* | *model prediction* | *50%-alpha overlay*. Class colours follow the palette in Figure 3. Vegetation (Trees, Dry Grass) and Sky are predicted with high spatial precision; the dominant failure mode is boundary ambiguity between Landscape, Dry Grass, and Ground Clutter in the mid-image transition zone.